

An efficient joint source-channel coding for a D-dimensional array

Ido Kanter, Haggai Kfir and Shahar Keren

Minerva Center and the Department of Physics, Bar-Ilan University, Ramat-Gan 52900, Israel
(July 2003)

An efficient joint source-channel (S/C) decoder based on the side information of the source and on the MN-Gallager Code over Galois fields, q , is presented. The dynamical posterior probabilities are derived either from the statistical mechanical approach for calculation of the entropy for the correlated sequences, or by the Markovian joint S/C algorithm. The Markovian joint S/C decoder has many advantages over the statistical mechanical approach, among them: (a) there is no need for the construction and the diagonalization of a $q \times q$ matrix and for a solution to saddle point equations in q dimensions; (b) a generalization to a joint S/C coding of an array of two-dimensional bits (or higher dimensions) is achievable; (c) using parametric estimation, an efficient joint S/C decoder with the lack of side information is discussed. Besides the variant joint S/C decoders presented, we also show that the available sets of autocorrelations consist of a convex volume, and its structure can be found using the Simplex algorithm.

I. INTRODUCTION

Source coding is a process for removing redundant information from the source information symbol stream. Suppose we have a bitmapped image, then converting the bitmap image to GIF, JPEG or any of the familiar image formats used on the web is a source coding process. Not only can images be coded, but also sound, video frames, etc., and compressing the stream of information is source coding.

Channel coding is a procedure for adding redundancy as protection into the information stream which is to be transmitted; in other words, channel coding can be regarded as adding protection to the transmission process. For example, a wireless communication channel is affected by many factors such as distance, speed at which either party is moving, weather, buildings, other users' unintentional interference, etc., so errors cannot be avoided. During the last decade engineers and also physicists have designed efficient error correction techniques such as Low-Density-Parity-Check-Codes (LDPC) [1–4] or Turbo [5] codes that nearly saturate Shannon's limit.

In a typical scenario of a communication channel there are two major resources which are highly limited. The first is power, which includes both transmitter power and receiver power. The second is bandwidth (channel capacity) indicating the speed at which the channel can transmit information, or more exactly, how many bps (bits per second). Both of these determine the capability of a channel. For example, by increasing the power we can reduce the error, but the power is limited. On the other hand, if the channel capacity is unlimited, we can just go ahead and add a large amount of protection (low rate), but again we cannot afford that since channel capacity is a commodity which in many scenarios is even more precious than power.

The main tradeoff in communication is the following: given a fixed capacity channel and a fixed amount of power, how should we allocate them between the source and the channel to get the best result, i.e, the smallest distortion? We know that a certain amount of channel capacity is allocated to the source and the rest is used for protection, but what is the ratio between them?

Shannon separation theorem states that source coding (compression) and channel coding (error protection) can be performed separately and sequentially, while maintaining optimality [6–9]. However, this is true only in the case of asymptotically long block lengths of data and point-to-point transmission. In many practical applications, the conditions of the Shannon's separation theorem neither holds, nor can it be used as a good approximation. Thus, considerable interest has developed in various schemes of joint source-channel (S/C) coding, where compression and error correction are combined into one mechanism (see, for instance, the following selected publications [10–15]).

The paper is organized as follows. In Section II Statistical Mechanical (SM) joint S/C coding is introduced, whereas in Section III the threshold of the code is calculated using scaling behavior for the required number of messages passing for the convergence of the algorithm [4,16,17]. In Section IV the efficiency of the SM joint S/C coding is compared to various separation schemes. A degradation in the performance of the SM joint S/C coding is examined in Section V as a function of the spectrum of the eigenvalues of the transfer matrix. In Section VI the Simplex algorithm is used to calculate the available space of a possible set of autocorrelations. The drawbacks of the SM joint S/C coding are discussed in Section VII, and advanced S/C coding is presented in Section VIII. The Markovian joint S/C coding and its efficiency are discussed in Section IX. Based on the parametric estimation methods the Markovian joint S/C

decoder with the lack of side information is discussed in Section X. Its extension to higher dimensions is discussed in Section XI. The paper closes with some concluding remarks.

II. JOINT S/C CODING - STATISTICAL MECHANICAL APPROACH

In our recent papers [18,17] a particular scheme based on a SM approach for the implementation of the joint S/C coding was presented and the main steps are briefly summarized below. The original boolean source is first mapped to a binary source [19,20] $\{x_i \pm 1\}$ $i = 1, \dots, L$, and is characterized by a finite set of autocorrelations bounded by the length k_0

$$C_{k_1, \dots, k_m} = \frac{1}{L} \sum_{i=1}^L x_i \prod_{j=0}^m x_{(i+k_j) \bmod L} \quad (1)$$

where $k_m \leq k_0$ is the highest length autocorrelation taken and the total number of possible different autocorrelations is 2^{k_0} . For $k_0 = 2$, for instance, there are only 4 possible correlations, C_0, C_1, C_2 and C_{12} , and for $k_0 = 3$ there are 8 possible different correlations; $C_0, C_1, C_2, C_3, C_{12}, C_{13}, C_{23}, C_{123}$, where we do not assume left-right symmetry for the source. Note that for the general k_0 and $m = 1$, eq. 1 is reduced to the two-point autocorrelation functions [21]. The number of sequences obeying these 2^{k_0} constraints is given by

$$\Omega = \text{Tr}_{\{x_i = \pm 1\}} \prod_{\{k_1, k_2, \dots, k_m\}} \delta\left(\sum_{i=1}^L x_i \prod_{j=0}^m x_{i+k_j} - LC_{k_1, \dots, k_m}\right) \quad (2)$$

where $m = 0$ stands for C_0 . Using the integral representation of the delta functions, eq. 2 can be written as

$$\begin{aligned} \Omega &= \int_{-\infty}^{\infty} \prod_{\{k_1, \dots, k_m\}} dy_{\{k_1, \dots, k_m\}} \exp\left(\sum y_{k_1, \dots, k_m} C_{k_1, \dots, k_m}\right) \\ &\text{Tr} \exp\left(\sum_{k_1, \dots, k_m} y_{k_1, \dots, k_m} \sum_i x_i \prod_{j=0}^m x_{i+k_j}\right) \end{aligned} \quad (3)$$

Since $k_j \leq k_0$, the last term of eq. 3 indicates that the trace can be performed using the standard transfer matrix (of size $2^{k_0} \times 2^{k_0}$) method [23]. More precisely, assume two successive blocks of k_0 binary variables denoted by (x_1, \dots, x_{k_0}) and $(x_{k_0+1}, \dots, x_{2k_0})$. The element (i, j) of the transfer matrix is equal to the value of the last exponential term (on the r.h.s of the trace) of eq. 3, where the first block is in state i (among 2^{k_0} possible states) and the second block is in state j . The transfer matrix is a non-negative matrix (as long as the y_{k_1, \dots, k_m} are real numbers), and the leading eigenvalue is positive and non-degenerate [23]. In the leading order one finds

$$\begin{aligned} \Omega &= \int dy_k \exp\{-L[\sum y_{k_1, \dots, k_m} C_{k_1, \dots, k_m} \\ &\quad - \ln \lambda_{max}(\{y_{k_1, \dots, k_m}\})]\} \end{aligned} \quad (4)$$

where λ_{max} is the maximal eigenvalue of the corresponding transfer matrix. For large L and using the saddle point method, the entropy, $H_2(\{C_{k_1, \dots, k_m}\})$, is given in the leading order by

$$\begin{aligned} H_2(\{C_{k_1, \dots, k_m}\}) &= \frac{1}{\ln 2} \left[\frac{1}{k_0} \ln \lambda_{max}(\{y_{k_1, \dots, k_m}\}) \right. \\ &\quad \left. - \sum_{k_1, \dots, k_m}^{k_0} y_{k_1, \dots, k_m} C_{k_1, \dots, k_m} \right] \end{aligned} \quad (5)$$

where $\{y_{k_1, \dots, k_m}\}$ are determined from the saddle point equations of Ω [17]. Assuming Binary Symmetric Channel (BSC) and using Shannon's lower bound, the channel capacity of sequences with a given set of autocorrelations bounded by a distance k_0 is given by

$$C = \frac{1 - H_2(f)}{H_2(\{C_{k_1, \dots, k_m}\}) - H_2(P_b)} \quad (6)$$

where f is the channel bit error rate and p_b is a bit error rate. The saddle point solutions derived from eq. 4 indicate that the equilibrium properties of the one-dimensional Ising spin system ($x_i = \pm 1$) with up to order k_0 multi-spin interactions [24]

$$H = - \sum_i \sum_{k=1}^{k_0} \frac{y_{k_1, \dots, k_m}}{\beta} x_i \prod_{j=0}^m x_{i+k_j} \quad (7)$$

obey in the leading order the autocorrelation constraints, eq. 1. This property of the effective Hamiltonian, eq. 7, is used in simulations to generate an ensemble of signals (source messages) with the desired set of autocorrelations. *Note that in the following we choose $\beta = 1$, and hence we denote $\{y_{k_1, \dots, k_m}\}$ as interactions.*

The transfer matrix method indicates that the relevant scale of the correlated source message is k_0 . Hence, our encoding/decoding procedure is based on the MN code [25] for a finite field $q = 2^{k_0}$ [26,28], which is based on the construction of two sparse matrices A and B of dimensionalities $L_0/R \times L_0$ and $L_0/R \times L_0/R$ respectively, where R is the code-rate and $L_0 = L/k_0$. The matrix $B^{-1}A$ is then used for encoding the message

$$t = B^{-1}Ax \pmod{\mathbf{q}} \quad (8)$$

The finite field message vector t is mapped to a binary vector and then transmitted. The received message, r , is corrupted by the channel bit error rate, f .

The decoding of symbols of k_0 successive bits (named in the following as a *block* of bits or binary variables) is based on the solution of the syndrome

$$Z = Br = Ax + Bn \pmod{\mathbf{q}} \quad (9)$$

where n stands for the corresponding noise of k_0 successive bits. The solution of the L_0/R equations with $L_0(1/R+1)$ variables is based on the standard message passing introduced for the MN decoder over Galois fields with $q = 2^{k_0}$ [26,28] and with the following modification. The horizontal pass is left unchanged, *but a dynamical set of probabilities assigned for each block is used in the vertical pass.* The Dynamical Block Probabilities (DBP), $\{P_n^c\}$, are determined following the current belief regarding the neighboring blocks and are given by

$$\begin{aligned} \gamma_n^c &= S_I(c) \left(\sum_{l=1}^q q_L^l S_L(l, c) \right) \left(\sum_{r=1}^q q_R^r S_R(c, r) \right) \\ P_n^c &= \frac{\gamma_n^c}{\sum_{j=1}^q \gamma_n^j} \end{aligned} \quad (10)$$

where $l/r/c$ denotes the state of the left/right/center ($n-1/n+1/n$) block respectively and q_L^l/q_R^r are their posterior probabilities. $S_I(c) = e^{-\beta H_I}$ stands for the Gibbs factor of the inner energy of a block, k_0 successive binary variables spins, characterized by an energy H_I at a state c , see eq. 7. Similarly $S_L(l, c)$ ($S_R(c, r)$) stands for the Gibbs factor of consecutive Left/Center (Center/Right) blocks at a state l, c (c, r) [17,18]. The complexity of the calculation of the block prior probabilities is $O(Lq^2/\log q)$ where $L/\log q$ is the number of blocks. The decoder complexity per iteration of the MN codes over a finite field q can be reduced to order $O(Lqu)$ [2,29], where u stands for the average number of checks per block. Hence the total complexity of the DBP decoder is of the order of $O(Lqu + Lq^2/\log q)$.

Another way to represent the dynamical behavior of the SM joint S/C decoder is in the framework of message passing on a graph. Typically, the graph is bipartite and consists of variable nodes and check nodes. A message from variables to checks is a horizontal pass, and a message from checks to variables is a vertical pass. In the SM joint S/C decoder there are *three* layers, as presented in Fig. 1. The first layer represents the checks and the second layer represents the variables, where each variable and check stands for a block of k_0 bits. The size of the third layer, denoted as dynamical block posterior probabilities derived from the Transfer Matrix (TM) method, is equal to the size of the source in blocks, $L_0 = L/k_0$. Each element in the third layer receives two arrows, representing the posterior probabilities of the neighboring blocks, and sends one output arrow to the center block, representing the current updated dynamical posterior probabilities which are then used for the vertical pass.

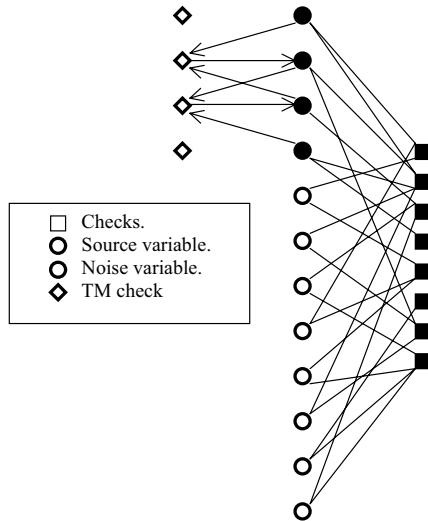


FIG. 1. A message passing in the SM joint S/C decoder is represented by a graph with the following three layers. The check blocks are represented by full squares, the full/open circles denote source/noise block variables and the open diamonds denote the calculators for the dynamical block posterior probabilities for the source block variables. Each one of these calculators receives an input message from its two neighbors (module L_0) and sends its output message to its block.

For simplification of the discussion below, in almost all of the simulation results we concentrate on rate $1/3$ and the construction of the matrices A and B follow reference [4] which is sketched in Fig. 2. The advantage of this construction is that the matrices A and B are very sparse, but the threshold of the code for large blocks is only $1 - 3\%$ from the channel capacity [4,16]. Furthermore, since B has a systematic structure, the complexity of the encoder scales linearly with L although B^{-1} is dense [30,31]. Of course, codes with higher thresholds exist (for instance in references [1,2]), hence the performance of the joint S/C algorithm reported below should be interpreted as a lower bound. (Results for a limited example with rate greater than one, $R > 1$, are briefly discussed in reference [35])

We conclude this section with the comment that the extension of the SM joint S/C algorithm in the framework of the MN-Gallager decoder to the Gallager decoder [32] is in question. In the Gallager decoder we first solve $L_0(1/R - 1)$ equations for the noise variables, and only in the final step is the message recovered. Since the noise is not spatially correlated, we do not see a simple way to incorporate in the Gallager case the side information about the spatial correlations among the message variables. The equivalence between these two (MN-Gallager and Gallager) similar decoders is in question.

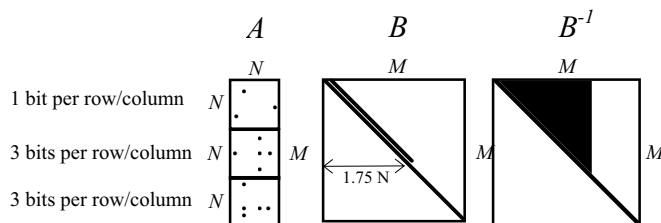


FIG. 2. The structure of the matrices A and B for the MN decoder taken from reference citeKS, for rate $1/3$. The black dots (area) denote the non-zero elements of the matrices A , B , B^{-1}

For illustration, in Fig. 3 we present results for rate $R = 1/3$, $L = 10,000$, $q = 4$ and 8 where the decoding is based on the dynamical block posterior probabilities, eq. 10, and with the following parameters. For $q = 4$ (open circles) $C_1 = 0.55$, $C_2 = 0.5$, $C_{12} = 0.4$ ($y_1 = 0.275$, $y_2 = 0.291$, $y_{12} = 0.422$) and $H_2 = 0.683$. Shannon's lower bound, eq. 6, is denoted by the double dotted line, where for $p_b = 0$ the channel noise level is $f_c = 0.227$. For $q = 8$ (open diamonds) $C_1 = 0.77$, $C_2 = 0.69$, $C_3 = 0.56$, $C_{123} = 0.7$ ($y_1 = 0.349$, $y_2 = 0.36$, $y_3 = 0.211$, $y_{123} = 0.443$) and $H_2 = 0.453$. Shannon's lower bound is denoted by the dashed line, where for $p_b = 0$ the channel noise level is $f_c = 0.275$. Each point was averaged over at least 1,000 messages. These results for both $q = 4$ and 8 indicate that the threshold of the presented decoder with $L = 10,000$ is $\sim 15\% - 20\%$ below the channel capacity for infinite source

messages.

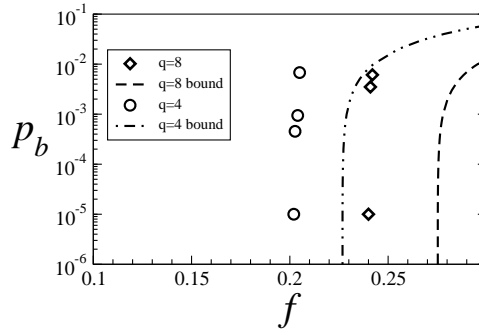


FIG. 3. Simulation results for rate $R = 1/3$, $L = 10,000$, $q = 4$ and 8 with the following parameters. For $q = 4$ (open circles) $C_1 = 0.55$, $C_2 = 0.5$, $C_{12} = 0.4$ ($y_1 = 0.275$, $y_2 = 0.291$, $y_{12} = 0.422$) and $H_2 = 0.683$. Shannon's lower bound, eq. 6, is denoted by the double dotted line. For $q = 8$ (open diamonds) $C_1 = 0.77$, $C_2 = 0.69$, $C_3 = 0.56$, $C_{123} = 0.7$ ($y_1 = 0.349$, $y_2 = 0.36$, $y_3 = 0.211$, $y_{123} = 0.443$) and $H_2 = 0.453$. Shannon's lower bound is denoted by the dashed line. Each point was averaged over at least 1,000 source messages with the desired set of autocorrelations.

III. THE THRESHOLD OF THE CODE

An interesting question is to measure the efficiency of the decoder, eq. 10, as a function of the maximal correlation length taken k_0 , the strength of the correlations, the size of the finite fields q and to compare the efficiency with the separation schemes. A direct answer to the questions raised is to implement exhaustive simulations on increasing source length, various finite fields q , and sets of autocorrelations, which result in the bit error probability versus the flip rate f . Besides the enormous computational time required, the conclusions would be controversial since it is unclear how to compare, for instance, the performance as a function of q ; with the same number of transmitted blocks or with the same number of transmitted bits.

In order to overcome these difficulties, for a given MN-Gallager code and with DBP decoding over $\text{GF}(q)$ and a set of autocorrelations, the threshold f_c for $L \rightarrow \infty$ is estimated from the scaling argument of the convergence time, which was previously observed for $q = 2$ [4,16]. The median number of message passing steps, t_{med} , necessary for the convergence of the MN-DBP algorithm is assumed to diverge as the level of noise approaches f_c from below. More precisely, we found that the scaling for the divergence of t_{med} is *independent of q* and is consistent with

$$t_{med} = \frac{A}{f_c - f} \quad (11)$$

where for a given set of autocorrelations and q , A is a constant. Moreover, for a given set of autocorrelations and a finite field q , the extrapolated threshold f_c is independent of L , as demonstrated in Fig. 4. This observation is essential to determine the threshold of a code based on the above scaling behavior. Note that the estimation of t_{med} is a simple computational task in comparison with the estimation of low bit error probabilities for large L , especially close to the threshold. We also note that the analysis is based on t_{med} instead of the average amount of message passing, t_{av} , [4] since we wish to prevent the dramatic effect of a small fraction of finite samples with slow convergence or no convergence. [33,34]

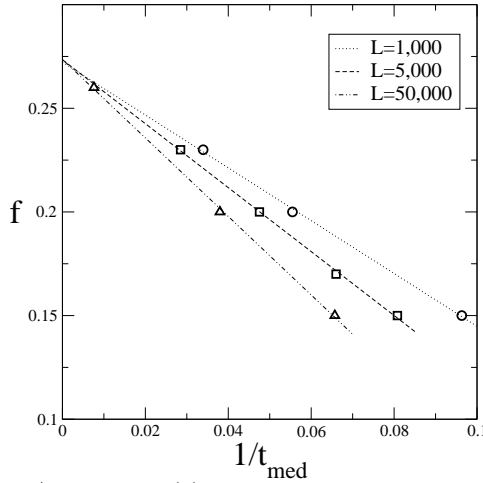


FIG. 4. The flip rate f as a function of $1/t_{med}$ for GF(4) with $C_1 = C_2 = 0.8$ and $L = 1,000, 5,000, 50,000$. The lines are a result of a linear regression fit. The threshold, $f_c \sim 0.272$, extrapolated from the scaling behavior eq. 11, is independent of N .

All simulation results presented below are derived for rate $1/3$ and the construction of the matrices A and B of the MN code are taken from [4]. In all examined sets of autocorrelations, $10^3 \leq L \leq 5 \times 10^4$ and $4 \leq q \leq 64$, the scaling for the median convergence time was indeed recovered. For illustration, in Fig. 5, we present the scaling behavior for the amount of message passing for the two examined cases presented in Fig. 3. (Note that this decoder can be extended to rate $R > 1$ and results for a limited example are presented in reference [35])

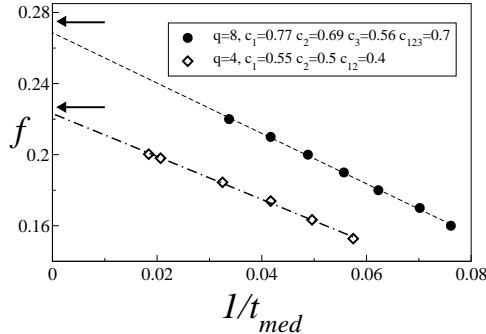


FIG. 5. The flip rate f as a function of $1/t_{med}$ for the two examined cases of Fig. 3. The extrapolated threshold for $q = 4, 8$ is $0.223, 0.265$, which are about 98% of the Shannon's lower bound $0.2267, 0.275$, respectively.

For a given set of autocorrelations, $\{C_{k_1, \dots, k_m}\}$ where $k_m \leq k_0$, the MN decoder, eq. 10, can be implemented with any field $q \geq 2^{k_0}$. In order to optimize the complexity of the decoder it is clear that one has to work with the minimal allowed field, $q = 2^{k_0}$. However, when the goal is to optimize the threshold of the code, the selection of the optimal field, q , is in question. To answer this question we present in Fig. 6 results for $k_0 = 2$ ($C_1 = C_2 = 0.86$) and $q = 4, 16, 64$. It is clear that the threshold, f_c , increases as a function of q as was previously found for the case of *i.i.d* sources. [26,27] More precisely, the estimated thresholds for $q = 4, 16, 64$ are $\sim 0.293, 0.3, 0.309$, respectively, and the corresponding Ratios ($\equiv f_c/f_{Sh}$) are $0.913, 0.934, 0.962$, where Shannon's lower bound $f_{Sh} = 0.321$. Note that the extrapolation of f_c for large q appears asymptotically to be consistent with $f_c(q) \sim 0.316 - 0.18/q$.

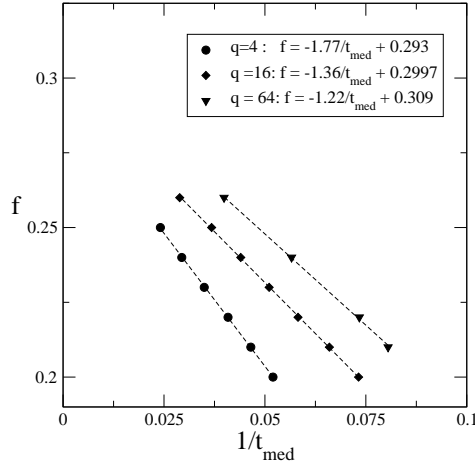


FIG. 6. The scaling behavior, f as a function of $1/t_{med}$, for $C_1 = C_2 = 0.86$ and $q = 4, 16, 64$. The lines are a result of a linear regression fit. The estimated thresholds for $q = 4, 16, 64$ are 0.293, 0.3, 0.309, and the corresponding $Ratio \equiv f_c/f_{Sh} = 0.913, 0.934, 0.962$, where $f_{Sh} = 0.321$.

IV. COMPARISON BETWEEN JOINT AND SEPARATION SCHEMES

Results of simulations for $q = 4, 8, 16$ and 32 and selected sets of autocorrelations are summarized in Table I (Fig. 7) and the definition of the symbols is: $\{C_k\}$ denotes the imposed values of two-point autocorrelations as defined in eqs. 1 and 2; $\{y_k\}$ are the interaction strengths, eq. 7; H represents the entropy of sequences with the given set of autocorrelations, eq. 5; f_c is the estimated threshold of the MN decoder with the DBP derived from the scaling behavior of t_{med} , eq. 11; f_{Sh} is Shannon's lower bound, eq. 6; $Ratio$ is the efficiency of our code, f_c/f_{Sh} ; Z_R indicates the gzip compression rate averaged over files of the sizes $10^5 - 10^6$ bits with the desired set of autocorrelations. We assume that the compression rate with $L = 10^6$ achieves its asymptotic ratio, as was indeed confirmed in the compression of files with different L ; $1/R^*$ indicates the ideal (minimal) ratio between the transmitted message and the source signal after implementing the following two steps: compression of the file using gzip and then using an *ideal optimal encoder/decoder*, for a given BSC with f_c . A number greater than (less than) 3 in this column indicates that the MN joint S/C decoder is more efficient (less efficient) in comparison to the channel separation method using the standard gzip compression. The last four columns of Table I (Fig. 7) are devoted to the comparison of the presented joint S/C decoder with advanced compression methods. PPM_R and AC_R represent the compression rate of files of the size $10^5 - 10^6$ bits with the desired autocorrelations using the Prediction by Partial Match [36] and for the Arithmetic Coder [37], respectively. Similarly to the gzip case, $1/R_{PPM}$ and $1/R_{AC}$ denote the optimal (minimal) rate required for the separation process (first a compression and then an ideal optimal encoder/decoder) assuming a BSC with f_c .

q	c_1	c_2	c_3	c_4	c_5	y_1	y_2	y_3	y_4	y_5	H	f_c	f_{Sh}	Ratio	Z_R	$\frac{1}{R^*}$	PPM_R	$\frac{1}{R_{PPM}}$	AC_R	$\frac{1}{R_{AC}}$
4	0.65	0.65	-	-	-	0.29	0.53	-	-	-	0.58	0.239	0.247	0.97	0.69	3.32	0.64	3.1	0.65	3.12
4	0.72	0.72	-	-	-	0.3	0.61	-	-	-	0.49	0.253	0.266	0.95	0.61	3.3	0.55	3.001	0.58	3.13
4	0.8	0.8	-	-	-	0.32	0.71	-	-	-	0.38	0.273	0.294	0.93	0.5	3.23	0.43	2.76	0.48	3.1
4	0.86	0.86	-	-	-	0.37	0.81	-	-	-	0.29	0.293	0.321	0.91	0.41	3.16	0.32	2.52	0.38	2.9
8	-0.65	0.6	-0.55	-	-	-0.31	0.23	-0.23	-	-	0.59	0.236	0.244	0.97	0.71	3.34	0.66	3.14	0.67	3.16
16	0.6	0.6	0.58	0.6	-	0.10	0.17	0.164	0.33	-	0.57	0.229	0.249	0.92	0.7	3.12	0.66	2.95	0.67	2.98
32	0.62	0.7	0.55	0.55	0.6	0.32	0.82	-0.44	-0.22	0.51	0.49	0.242	0.266	0.91	0.62	3.06	0.56	2.77	0.6	2.96

FIG. 7. Results for $q = 4, 8, 16, 32$ and selected sets of two-point autocorrelations $\{C_k\}$

Table I indicates the following main results: (a) For $q = 4$ (the upper part of Table I) a degradation in the performance is observed as the correlations are enhanced, and as a result the entropy decreases. The degradation appears to be significant as the entropy is below ~ 0.3 (or for the test case $R = 1/3$, $f_c \geq 0.3$). [38] A similar degradation was also observed for larger values of q as the entropy decreases. (b) The efficiency of our joint S/C coding technique is superior to the alternative standard gzip compression in the S/C separation technique. For high entropy the gain of the MN decoder is about 5–10%. This gain disappears as the entropy and the performance of the

presented decoder, eq. 10, are decreased. (c) In comparison to the standard gzip, the compression rate is improved by 2–5% using the AC method. A further improvement of a few percent is achieved by the PPM compression. This latter improvement appears to be significant in the event of low entropy. (d) With respect to the performance, the presented joint S/C decoder, eq. 10, appears to be comparable with the presented separation methods, but for low entropy it appears that the PPM compression is superior. However, one should bear in mind a better threshold for the MN code can be found by optimizing the code [1]. (e) With respect to the computational time of the S/C coding, our limited experience indicates that the joint S/C decoder is faster than the AC separation method and the PPM separation method is substantially slower. Finally, we note that using the side information, the set of autocorrelations, one can design a special compression procedure which may overcome the disadvantages of the abovementioned compression methods [42].

V. THE ROLE OF THE SPECTRUM OF EIGENVALUES

For a given q , there are many sets of autocorrelations, $\{C_{k_1, \dots, k_m}\}$, in q dimensions obeying the same entropy (see the discussion in section VI below). An interesting question is whether the performance of the presented MN decoder measured by the Ratio ($\equiv f_c/f_{Sh}$) is a function of the entropy only. Our numerical simulations indicate that the entropy is not the only parameter which controls the performance of the algorithm. For the same entropy and q the Ratio can fluctuate widely among different sets of correlations. For illustration, in Table II (Fig. 8) results for two sets of autocorrelations with *the same entropy* are summarized for each $q = 4, 8, 16$ and 32 . It is clear that as the Ratio ($\equiv f_c/f_{Sh}$) is much degraded the gzip performance is superior (the second example with $q = 8$ and 32 in Table II (Fig. 8) where the Ratio is 0.8 and 0.72, respectively). The crucial question is to find the criterion to classify the performance of the algorithm among all sets of autocorrelations obeying the same entropy. Our generic criterion is *the decay of the correlation function over distances beyond two successive blocks*. However, before examination of this criterion, we return to some aspects of statistical physics.

The entropy of sequences with a given set of autocorrelations bounded by a distance $k_0 = \log_2(q)$ is determined via the effective Hamiltonian consisting of q interactions, eq. 7. As a result the entropy of these sequences is *the same* as the entropy of the effective Hamiltonian, $H\{y_{k_1, \dots, k_m}\}$, at the inverse temperature $\beta = 1$, eq. 5. As for the usual scenario of the transfer matrix method, the leading order of quantities such as free energy and entropy are a function of the *largest eigenvalue* of the transfer matrix only. On the other hand the decay of the correlation function is a function of the whole spectrum of the $q = 2^{k_0}$ eigenvalues (and eigenvectors) [23]. Asymptotically, the decay of the correlation function is determined from the ratio between the second largest eigenvalue, λ_2 , and the largest eigenvalue, λ_2/λ_{max} . From the statistical mechanical point of view, one may wonder why the first q correlations can be determined using the information of λ_{max} only. The answer is that once the transfer matrix is defined as a function of $\{y_{k_1, \dots, k_m}\}$, eqs. 3-7, *all eigenvalues* are determined as well as λ_{max} . There is no way to determine λ_{max} independently of all other eigenvalues.

In Table II (Fig. 8) results of the MN decoder, eq. 10, for $q = 4, 8, 16, 32$ are presented. For each q , two different sets of autocorrelations characterized by the *same entropy* and threshold f_{Sh} are examined. The practical method we used to generate different sets of autocorrelations with the same entropy was a simple Monte Carlo over the space of $\{C_{k_1, \dots, k_m}\}$ [39]. The additional column in Table II (in comparison with Table I) is the ratio between λ_2/λ_{max} , which characterizes the decay of the correlation function over large distances. It is clear that for a given entropy as λ_2/λ_{max} increases/decreases, the performance of the joint S/C decoder measured by the Ratio f_c/f_{Sh} is degraded/enhanced, independent of q . The new criterion to classify the performance of the decoder among all sets of autocorrelations obeying the same entropy is the decay of the correlation function. This criterion is consistent with the tendency that as the first k_0 two-points autocorrelations are increased/decreased a degradation/enhancement in the performance is observed (see Table I). The physical intuition is that as the correlation length increases, the relaxation time to the equilibrium macroscopic state increases, and flips on larger scales than nearest neighbor blocks are required. Finally, we note that in the general scenario, the first two largest eigenvalues are not sufficient to approximate the correlation function on short length scales and the comparison of the efficiency of the decoder should take into account the entire spectrum of eigenvalues and the eigenvectors [23].

q	c_1	c_2	c_3	c_4	c_5	y_1	y_2	y_3	y_4	y_5	λ_2/λ_{max}	H	f_c	f_{Sh}	Ratio	Z_R	$\frac{1}{R^*}$
4	0.785	0.636	—	—	—	0.88	0.11	—	—	—	0.65	0.49	0.256	0.266	0.97	0.61	3.48
4	0.499	0.769	—	—	—	0.091	0.921	—	—	—	0.83	0.49	0.242	0.266	0.91	0.61	3.01
8	0.77	0.69	0.561	—	—	0.544	0.598	-0.167	—	—	0.59	0.48	0.259	0.269	0.96	0.6	3.42
8	0.557	0.577	0.75	—	—	-0.04	0.218	0.774	—	—	0.86	0.48	0.215	0.269	0.80	0.62	2.47
16	0.721	0.489	0.353	0.303	—	1.247	-0.212	-0.149	0.169	—	0.4	0.57	0.241	0.249	0.97	0.68	3.32
16	0.6	0.6	0.58	0.6	—	0.104	0.17	.164	0.327	—	0.82	0.57	0.229	0.249	0.92	0.7	3.12
32	0.62	0.7	0.55	0.55	0.599	0.324	0.821	-0.438	-0.219	0.51	0.78	0.49	0.242	0.266	0.91	0.62	3.06
32	0.5	0.62	0.5	0.6	0.669	-0.159	0.351	-0.266	0.366	0.66	0.89	0.49	0.191	0.266	0.72	0.64	2.26

FIG. 8. Results for $q = 4, 8, 16, 32$ and different sets of two-point autocorrelations. For each q , two different sets of two-point autocorrelations characterized by the same entropy and threshold f_{Sh} are examined. As λ_2/λ_{max} increases/decreases, the performance of the joint S/C decoder measured by the Ratio f_c/f_{Sh} is degraded/enhanced.

Note that the decay of the correlation function in the intermediate region of a small number of blocks is a function of all the 2^{k_0} eigenvalues. Hence, in order to enhance the effect of the fast decay of the correlation function in the case of small λ_2/λ_{max} , we also try to enforce in our Monte Carlo search that all other $2^{k_0} - 2$ eigenvalues be less than $A\lambda_{max}$ with the minimal possible constant A . This additional constraint was easily fulfilled for $q = 4$ with $A = 0.1$, but for $q = 32$ the minimal A was around 0.5.

VI. POSSIBLE SETS OF AUTOCORRELATIONS AND THE SIMPLEX ALGORITHM

The entropy of correlated sequences can be calculated from eq. 5. For the simplest case of sequences obeying only C_1 and C_2 the numerical solution of the saddle point equations indicate that the entropy is non-zero only in the regime

$$-(1 + C_2)/2 \leq C_1 \leq (1 + C_2)/2 \quad (12)$$

where out of this regime the entropy is zero. The boundaries, $C_1 = |(1 + C_2)/2|$, are characterized by the following phenomena: (a) the entropy falls abruptly to zero at the boundary, and (b) y_1 and $-y_2$ diverge at the boundary (the one-dimensional Hamiltonian, eq. 7 consists of frustrated loops).

These limited results obtained from the numerical solutions of the saddle point equations suffer from the following limitations: (a) finding the boundaries of the regime in the spaces of $\{C_{k_1, \dots, k_m}\}$ with a finite entropy is very sensitive to the numerical precision since on the boundary $\{|y_i|\}$ diverge; (b) it is unclear whether the available space consists of a connected regime; (c) the question of whether out of the space with a finite entropy, there are a finite or infinite number of sequences (for instance $e^{\sqrt{L}}$) obeying the set of autocorrelations cannot be answered using the saddle point method; (d) extension of the saddle point solutions to identify the boundaries of the finite entropy regime to many dimensions is a very heavy numerical task.

To overcome these difficulties and to answer the above questions, we show below how the possible sets of autocorrelations can be identified using the Simplex algorithm.

For the case of only two constraints C_1 and C_2 , for instance, let us concentrate on three successive binary variables S_i, S_{i+1}, S_{i+2} , where $S_i = \pm 1$. Since the Hamiltonian, eq. 7, obeys in this case an inversion symmetry, let us examine only the 4 configurations out of 8 where $S_2 = -$, $(\pm, -, \pm)$. For these 4 configurations one can assign the following marginal probabilities, $P(\pm, -, \pm)$, where each probability stands for the fraction of sequences obeying C_1 and C_2 with a given state for these three successive binary variables. In the SM language we measure the probabilities of these four states in thermal equilibrium of the micro-canonical ensemble obeying eq. 1. It is clear that the Hamiltonian, eq. 7, is translationally invariant, $P(S_i, S_{i+1}, S_{i+2})$ is independent on i after averaging over all sequences obeying the constraints of eq. 1.

For these 4 marginal probabilities one can write the following 8 equations, see eq. 15. For a given C_1 , these 8 equations and inequalities can be solved for the minimum and the maximum available C_2 using the Simplex method. Running over values of $-1 \leq C_1 \leq 1$, we indeed recover the result of eq. 12. However, the *Simplex solution indicates the lack of even finite sequences beyond the regime with finite entropy*. Hence simple geometrical calculation of constraint 12 indicates that the fraction of the space (C_1, C_2) with available sequences is 1/2.

For the case of three constraints, C_1, C_2 and C_3 , one can similarly write the following 15 equalities and inequalities for the 8 probabilities of 4 successive binary variables $P(\pm, \pm, -, \pm)$, see eq. 16.

For a given C_1 and C_2 , these 15 equations and inequalities can be solved for the minimum and the maximum available C_3 using the Simplex method. The Simplex solution indicates: (a) the available solution in the three-dimensional box $(-1 : 1, -1 : 1, -1 : 1)$ for (C_1, C_2, C_3) is a connected region bounded by a few plans whose detailed equations will be given elsewhere [40]; (b) the fraction of the volume of the box with a positive number of sequences obeying the three constants is ~ 0.222 . Preliminary results indicate that for 4 ($C_i, i = 1, 2, 3, 4$) and 5 ($C_i, i = 1, 2, 3, 4, 5$) constraints the available volume is $\sim 0.085, 0.034$, respectively.

The fraction of possible sets of autocorrelations appears to decrease as the number of constraints increases. However, the question of whether the fraction of available autocorrelations drops exponentially with the number of constraints as well as its detailed spatial shape is the subject of our current research [40].

We conclude the discussion in this section with the following general result [42]. The available volume for the general case of q constraints $\{C_{k_1, \dots, k_m}\}$ $k_m < \log_2(q)$ is convex. The main idea is that one can verify that the set of equalities can be written in a matrix representation in the following form

$$\mathbf{M}P = C \quad (13)$$

where \mathbf{M} is a matrix with elements ± 1 ; P represents the marginal probabilities $P(\pm, \pm, \dots)$ and C represents the desired correlations or a normalization constant (for instance $C_1/2, C_2/2$ and $1/2$, for the case of eq. 15). The inequalities force the probabilities into the range $[0 : 1]$. Clearly if $P_1(\pm, \pm, \dots)$ and $P_2(\pm, \pm, \dots)$ are two sets of probabilities obeying eq. 13 then

$$\lambda P_1 + (1 - \lambda)P_2 \quad (14)$$

is also a solution of the set of the equalities ($0 \leq \lambda \leq 1$). Hence, the available volume is convex.

$$\begin{aligned} P(-, -, +) + P(-, -, -) - P(+, -, +) - P(+, -, -) &= C_1/2 \\ P(+, -, -) + P(-, -, -) - P(+, -, +) - P(-, -, +) &= C_1/2 \\ P(-, -, +) + P(-, -, -) + P(+, -, +) + P(+, -, -) &= 1/2 \\ P(+, -, +) + P(-, -, -) - P(+, -, -) + P(-, -, +) &= C_2/2 \\ 0 \leq P(\pm, -, \pm) &\leq 1 \end{aligned} \quad (15)$$

$$\begin{aligned} &P(+, +, -, +) + P(+, +, -, -) + P(-, -, -, +) + P(-, -, -, -) \\ &- P(+, -, -, +) - P(+, -, -, -) - P(-, +, -, +) - P(-, +, -, -) = C_1/2 \\ &P(+, -, -, +) + P(+, -, -, -) + P(-, -, -, +) + P(-, -, -, -) \\ &- P(+, +, -, +) - P(+, +, -, -) - P(-, +, -, +) - P(-, +, -, -) = C_1/2 \\ &P(+, +, -, -) + P(+, -, -, -) + P(-, +, -, -) + P(-, -, -, -) \\ &- P(+, +, -, +) - P(+, -, -, +) - P(-, +, -, +) - P(-, -, -, +) = C_1/2 \\ &P(-, +, -, +) + P(-, +, -, -) + P(-, -, -, +) + P(-, -, -, -) \\ &- P(+, +, -, +) - P(+, +, -, -) - P(+, -, -, +) - P(+, -, -, -) = C_2/2 \\ &P(+, +, -, +) + P(+, -, -, -) + P(-, +, -, +) + P(-, -, -, -) \\ &- P(+, +, -, -) - P(+, -, -, +) - P(-, +, -, -) - P(-, -, -, +) = C_2/2 \\ &P(+, +, -, +) + P(+, -, -, +) + P(-, +, -, -) + P(-, -, -, -) \\ &- P(+, +, -, -) - P(+, -, -, -) - P(-, +, -, +) - P(-, -, -, +) = C_3/2 \\ &P(+, +, -, +) + P(+, -, -, -) + P(-, +, -, +) + P(-, -, -, -) \\ &+ P(+, +, -, -) + P(+, -, -, +) + P(-, +, -, -) + P(-, -, -, +) = 1/2 \\ &0 \leq P(\pm, \pm, -, \pm) \leq 1 \end{aligned} \quad (16)$$

VII. DRAWBACKS OF THE SM APPROACH

The presented joint S/C decoder based on the SM approach suffers from the following drawbacks: (a) For each transmitted block one must calculate a $q \times q$ matrix, where each element of this matrix is a function of all q autocorrelations, $\{C_{k_1, \dots, k_m}\}$. Hence, the naive complexity of the construction of the transfer matrix is $O(q^4)$. Furthermore, for

each transmitted block the complexity of the calculation of the leading eigenvalue of the transfer matrix is of $O(q^3)$. (b) The required memory is of the order $O(q^2)$, where, for instance, for $K_0 = 20$ it results in a 1Mega Bytes. (c) The solution of the saddle point equations, eqs. 4-5, requires the calculation many times and with high precision of the leading eigenvalue of $q \times q$ matrix. From our experience, the calculation with high precision of the saddle point equations in $q = 2^{k_0}$ dimensions, $\{y_{k_1, \dots, k_m}\}$ is a heavy numerical task for $k_0 \geq 4$. (d) The extension of the decoder based on the SM approach to include an array of bits in two or a higher number of dimensions is impossible, since the trace in eq. 2 can be done only for very limited two-dimensional cases [23].

VIII. JOINT S/C DECODER WITH ADVANCED THRESHOLD

In order to overcome some of the abovementioned difficulties we present in this section a decoder with an advanced threshold, where the decoder gains from fluctuations among different finite source messages. For a given sequence of L bits, $\{x_1, x_2, \dots, x_L\}$, and $k_m \leq k_0$, there are $L_0 = L/k_0$ blocks, denoted by $\{A_1, A_2, \dots, A_{L_0}\}$. For a given finite field $q = 2^{k_0}$ we denote the number of possible different blocks by B_m $m = 1, 2, \dots, q$. In the first step of the algorithm, the probability of occurrence of all three possible successive blocks is calculated

$$\hat{P}(B_i, B_j, B_k) \equiv \frac{1}{L_0} \sum_{m=1}^{L_0} \delta_{A_m, B_i} \delta_{A_{m+1}, B_j} \delta_{A_{m+2}, B_k} \quad (17)$$

where we assume periodic boundary conditions. Note that although the number of possible triplets of blocks is 2^{3k_0} , the complexity of this step for a given source message scales linearly with L . [43]

The number of non-zero probabilities of occurrence of triplets is bounded from above by L_0 . However, in a typical scenario of some enhanced autocorrelations the number of non-zero $\hat{P}(B_i, B_j, B_k)$ is expected to be $\ll L_0$. Hence in the regime where $q^3 \gg L_0$ most of the $\hat{P}(B_i, B_j, B_k)$ are equal to zero, and the tensor, $\hat{P}(B_i, B_j, B_k)$, can be efficiently kept as a very sparse tensor. The sparseness of the tensor is expected even for long sequences, for instance, for $L = 10^5$ and $q = 128$ ($k_0 = 7$) $128^3 \gg 10^5/7$. In the following we discuss the importance of this observation.

The decoding of symbols of k_0 successive bits is again based on the standard message passing introduced for the MN decoder over Galois fields with $q = 2^{k_0}$ [26] and with the following modification. The horizontal pass is left unchanged, *but a dynamical set of probabilities assigned for each block is used in the vertical pass*. The Dynamical Block Probabilities (DBP), $\{P_n^c\}$, are determined following the current belief regarding the neighboring blocks in the following way

$$\gamma_n^{B_m} = \sum_{i,j=1}^q \frac{\hat{P}(B_i, B_m, B_j)}{\sum_{b=1}^q \hat{P}(B_i, b, B_j)} q_{m-1}^i q_{m+1}^j \quad (18)$$

$$\hat{P}_n^{B_m} = \frac{\gamma_n^{B_m}}{\sum_{j=1}^q \gamma_n^j} \quad (19)$$

where q_{m+1}^i/q_{m-1}^j stands for the posterior probabilities of the right/left block in the state i/j .

We compared the performance of this decoder with the performance of the previously discussed decoder based on the SM approach, eq. 10, for different values of q and with rate 1/3 where the construction of the matrices A and B again follows [4]. Results of the bit error rate, P_b , versus the channel bit error rate, f for $q = 8$, and a given set of autocorrelations are presented in Fig. 9, and for a set of autocorrelations with $q = 16$ in Fig. 10. It is clear that the threshold of the decoder based on eq. 18 is superior to the decoder based on the SM approach, eq. 10.

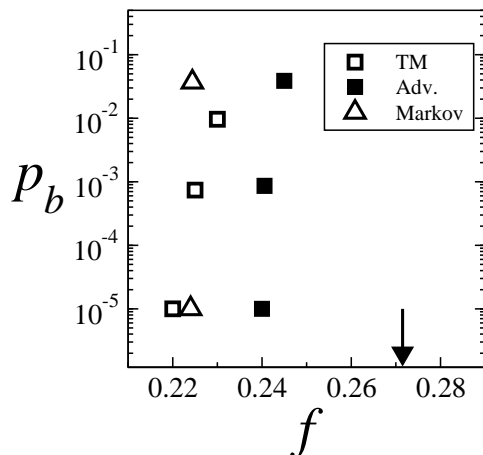


FIG. 9. The bit error rate, p_b versus the channel bit error rate f for $L = 10,000$, $R = 1/3$, $q = 8$ with $C_1 = C_2 = C_3 = 0.7$. Decoding following the dynamical block probabilities defined in eq. 10 (open squares), decoding following the advanced joint S/C decoder, eq. 18 (full squares) and decoding following the Markovian decoder, eq. 21 (open triangular). Each point is averaged over at least 1,000 source messages. Shannon's lowered bound, $f_c = 0.271$, derived from eq. 6 is denoted by an arrow.

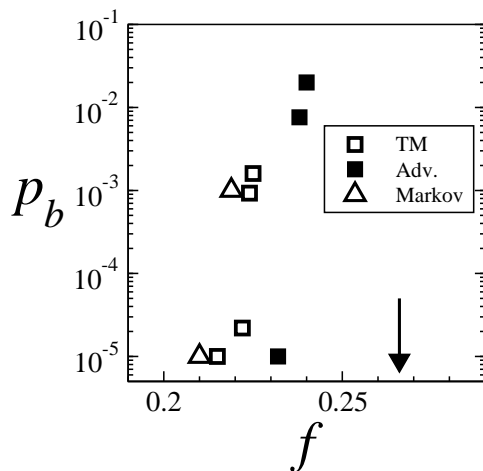


FIG. 10. The bit error rate, p_b versus the channel bit error rate f for $L = 10,000$, $R = 1/3$, $q = 16$ with $C_1 = 0.68$, $C_2 = 0.68$, $C_3 = 0.6$, $C_4 = 0.655$. Decoding following the dynamical block probabilities defined in eq. 10 (open squares), decoding following the advanced joint S/C decoder, eq. 18 (full squares) and decoding following the Markovian decoder, eq. 21 (open triangular). Each point is averaged over at least 1,000 source messages. Shannon's lowered bound, $f_c = 0.266$, derived from eq. 6 is denoted by an arrow.

Note that for finite L the dynamical block posterior probabilities defined in eq. 18 ($\hat{P}(B_i, B_j, B_k)$) fluctuate among

different samples, where for the decoder based on the SM approach, eq. 10, these probabilities are sample independent. This is one of the sources of the superiority of the presented decoder over the SM approach (at least for finite L).

Note also that the presented decoder, eq. 18, takes into account all higher order correlations (q autocorrelations, $\{C_{k_1, \dots, k_m}\}$) in a direct measure – the probability of occurrence of triplets of blocks, $\hat{P}(B_i, b, B_j)$. There is no need, as required in the SM approach, eq. 10, to calculate the form of a $q \times q$ matrix, to diagonalize large transfer matrices or to seek a saddle point in a large number of dimensions, q .

It is clear that the threshold of the advanced joint S/C decoder, eq. 18, is superior to the decoder based on the SM approach. However, from a practical point of view the advanced joint S/C decoder, eq. 18, suffers from the following disadvantages. Firstly, the complexity per message passing scales with $L_0 q^3$ (see eq. 18), where the complexity of the previously discussed algorithm is only $L_0 q^2$. Secondly, the size of the header (the transmitted side information, namely, the measured probabilities of occurrence of triplets of successive blocks) scales also with q^3 . Although the size of the header does not scale with L , it is a critical overhead for a finite L . In the following sections we show how to overcome these difficulties and to sail towards a practical algorithm in the large q limit.

IX. MARKOVIAN JOINT S/C DECODER

The calculation of the entropy using the transfer matrix methods indicates that the ensemble of sequences obeying in the leading order a given set of autocorrelations can also be derived using a Markovian process [22]. More precisely, the elements of the transition matrix, $\{P_{ij}\}$ (a transition from state i to j), are related to the transfer matrix elements, $\{T_{ij}\}$, via the following normalization

$$P_{ij} = \frac{T_{ij}}{\sum_j T_{ij}} \quad (20)$$

Using this analogue, one can now approximate the measured probability of occurrence of any q^3 combinations of three successive blocks, (A, B, C) , using the following formula:

$$\hat{P}(A, B, C) = \frac{\hat{P}(A, B)\hat{P}(B, C)}{\hat{P}(B)} \quad (21)$$

Hence, the dynamical block probabilities, eq. 10, can be now calculated with a complexity of q^2 , and the overall complexity of the Markovian joint S/C decoder per message passing is $O(Lq^2/\log(q))$. Note again that there is no need, as required in the SM approach, eq. 10, to calculate the form of a $q \times q$ matrix, to diagonalize large transfer matrices or to seek a saddle point in a large number of dimensions, q .

Note that in the limit of infinite L , eq. 21 is exact in the leading order of L . For a finite L , some corrections are expected. The deviation from a direct measure of the probability of occurrence of three successive blocks to the estimation of the r.h.s of eq. 21 is expected to be significant only for triplets with very low probability of occurrence (for instance, if the l.h.s of eq. 21 indicates that a triplet of three successive blocks is absent in a given sequence where the r.h.s makes one appearance). However, we do not expect these events with very low probabilities to dramatically affect the performance of the algorithm. This expectation was indeed confirmed in our simulations. Results are exemplified in Figs. 9 and 10, where the performance of the Markovian S/C decoder is compared with the SM approach, eq. 10. The difference in the threshold between these two methods is negligible for the examined cases.

The complexity of our Markovian S/C decoder was reduced to $O(L_0 q^2)$ per message passing. However, there is still a need for the transmission of the side information consisting of the measured probabilities of occurrence of all successive pairs of blocks, $\{\hat{P}(A, B)\}$. Hence the size of the header is of the order of $O(q^2)$. For $L \rightarrow \infty$ or more precisely for $L \gg q^2$ the overhead of the transmitted side information is negligible; however, for a finite $L \leq q^2$ it may cancel the benefits of the Markovian joint S/C decoder.

One way to reduce the overhead of the header of the order $O(q^2)$ is to transmit only the dominated elements of the matrix $\hat{P}(A, B)$. The remaining elements of the matrix are determined in the following way. Let us denote the sum of the transmitted dominated elements in the i th row by M_i and their number by N_i . The non-transmitted elements in each row are set equally to $(1 - M_i)/(q - N_i)$. It is clear that as we increase $\{N_i\}$ the structure of the approximated matrix converges to the true one. For sequences with enhanced autocorrelations the structure of the matrix $\hat{P}(A, B)$ was observed to be dominated by a small number of large elements. The result of simulations for $q = 8$ where the number of transmitted elements, $\sum M_i = 8$ (out of $q^2 = 64$), is presented in Fig. 11 and for the case of $q = 16$ where $\sum M_i = 16$ (out of $q^2 = 256$) is presented in Fig 12. The performance seems to be only slightly affected by this approximation, which dramatically reduces the required transmitted side information.

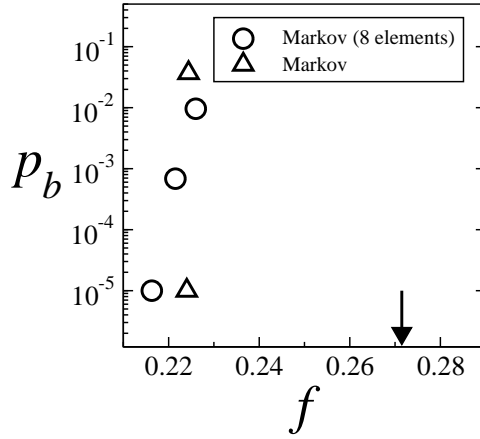


FIG. 11. The bit error rate, p_b versus the channel bit error rate f for $L = 10,000$, $R = 1/3$, $q = 8$ with $C_1 = C_2 = C_3 = 0.7$. Decoding following the Markovian process, eq. 21 (open triangle), decoding following the Markovian process where only 8 dominated elements of the transition matrix, $\hat{P}(A, B)$, are taken as a side information, and the rest of the elements are set equal to a constant such that the sum of each row is equal to 1 (open circle). Shannon's lower bound, $f_c = 0.271$, is denoted by an arrow.

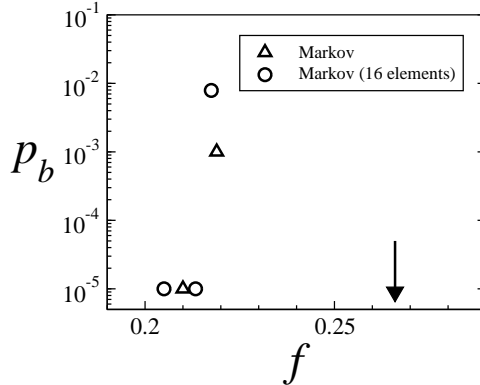


FIG. 12. The bit error rate, p_b versus the channel bit error rate f for $L = 10,000$, $R = 1/3$, $q = 16$ with $C_1 = 0.68$, $C_2 = 0.68$, $C_3 = 0.6$, $C_4 = 0.655$. Decoding following the Markovian process, eq. 21 (open triangular) and decoding following the Markovian process where only 16 dominated elements of the transition matrix, $\hat{P}(A, B)$, are taken as a side information, and the rest of the elements are set equal to a constant such that the sum of each row is equal to 1 (open circle). Shannon's lower bound, $f_c = 0.266$, is denoted by an arrow.

An interesting open question is the effect of use of the sparseness of the tensor $\hat{P}(B_i, B_j, B_k)$ on the average and the distribution of the number of required message passing for convergence of the decoding process.

X. EFFICIENT JOINT S/C DECODER WITH THE LACK OF SIDE INFORMATION

The discussion in the previous sections indicates that the performance of the presented joint S/C coding is not too far from Shannon's lower bound and, most probably, using an optimized code (a better construction for the matrices A and B of the MN code), the channel capacity can be nearly saturated. However for a finite block length the main drawback of our algorithm is the overhead of the header which must be encoded and transmitted reliably. One has to remember that the size of the header scales with q^2 where the precision of each element is of the order $O(\log L)$. This overhead is especially intolerable in the limit where

$$\frac{q^2 \log(L)}{L} \sim O(1) \quad (22)$$

Note that this is indeed the situation even for very large messages, $L = 10^6$, and the largest taken autocorrelation length is only $\log_2 q = 8$. The l.h.s of eq. 22 with these parameters is around 1.

In this section we explain how the abovementioned Markovian joint S/C can be implemented without the transmission of any side information, $\{y_{k_1, \dots, k_m}\}$ of eq. 5, or $\hat{P}(A, B)$ of eq. 21. The main idea can be easily exemplified in the framework of the Gallager code, where only at the end of the discussion do we extend it to the MN code.

The first N received bits (the source message) using the Gallager code with systematic parity-check matrix is the message itself which is generated by a Markovian process plus the additional channel noise f . Hence, from the receiver point of view the generator of the first N received bits is a Hidden Markov Process. The first task of the receiver is to estimate $\hat{P}(A, B)$ from the knowledge of the noisy received source message and the channel flip rate f . This type of *parametric estimation* is a common problem in statistics and can be solved (exactly or approximately) using the EM algorithm or by one of its variants [41]. More precisely, for an infinite source, $L \rightarrow \infty$, the transition matrix eq. 20 (or the interaction strengths eq. 5) can be recovered within a bounded error with $O(L)$ time complexity. For a finite L sequence the parameters of the Markovian process can be estimated approximately with an error of the order $O(q^2/L)$. Hence, the required parameters for the presented joint S/C decoder based on the dynamical block posterior probabilities can be estimated from the received noisy message. Note that as explained above, the error in the dominated elements of the transition matrix, $\hat{P}(A, B)$, is the most important ingredient for the performance of our joint S/C decoder, hence one may desire an efficient algorithm to estimate especially the dominated part of the transition matrix.

The critical problem with the above description is that our efficient decoder can be implemented only by the MN algorithm, where the decoder *simultaneously* estimates the values for the source and noise bits. In contrast, in the Gallager decoder, the values for the noise bits are firstly estimated, and only in the next step are the source bits recovered. Hence, the dynamical block posterior probabilities cannot be used (to our current knowledge) in the framework of the Gallager algorithm. Since in the MN decoder the source is not transmitted by itself, the question now is how to estimate the parameters of the Markovian process which are responsible for generating of the source message from the received message. Nevertheless, as explained below, this problem can be solved also for the MN case in $O(L)$ time complexity.

Let us first explain the solution for the examined MN construction, Fig. 2, then later sketch the general solution. For the used MN construction, Fig. 2, the first N rows of A are characterized by one non-zero element per row and column, where the first N rows of B are characterized by 2 non-zero elements (furthermore, each row of B cannot be written as a linear combination of the other rows). Hence, the first N bits of the syndrome, eq. 9, are equal to the source with an effective flip rate equal to $f_{eff} = 2f(1 - f)$. The EM algorithm with f_{eff} can now be used to estimate the finite number of parameters of the Markovian process generating the sequence.

For the general construction of the NM algorithm one adds/subtracts rows of the concatenated matrix $[A, B]$ and the corresponding received message bits Z (see eq. 9), such that a situation is finally reached as follows. The first N rows of A are the identity matrix, regardless of the construction of the first N rows of B , and with the corresponding Z_{eff} . From the knowledge of the noise level f and the structure of i th row of B one can now calculate the effective noise level, $f_{i,eff}$, of the i th received source bit. Note that all N effective noise, $\{f_{i,eff}\}$ are functions of a unique noise level f , and one can again estimate the parameters of the Markovian process using some variants of the EM algorithm. The only approximation used in the calculation of $\{f_{i,eff}\}$ *in the general case* is that the new form of the first N rows of B contain loops, hence $\{f_{i,eff}\}$ are correlated. However, these correlations are assumed to be small as the typical loops are of the order of $O(\log(L))$.

XI. MARKOVIAN JOINT S/C CODING IN HIGHER DIMENSIONS

The decoder based on the SM approach, eq. 10, is limited to a one-dimensional stream of bits, since the trace in eq. 3 can be done using the transfer matrix method (or any known method) only to very limited cases of a two-dimensional array of bits [23]. The analytical solution of a two-dimensional Ising system with arbitrary strength of even nearest neighbor interactions is not known and in three dimensions no analytical solution is known. On the contrary, the one-dimensional Markovian joint S/C decoder can be easily extended to a joint S/C coding of a two-dimensional array of bits or even to an array of bits in higher dimensions.

For illustration, assume that we have a two-dimensional picture to transmit using a joint S/C mechanism via a noisy channel. A simple way would be to convert the two-dimensional picture into a one-dimensional sequence and then to use, for instance, one of the abovementioned decoders. However, it is clear that the mapping of the two-dimensional picture into a one-dimensional sequence is not unique and of course the natural two-dimensional correlations are destroyed in this mapping (at least for the realistic case of finite k_0). An alternative way is to generalize the advanced threshold joint S/C decoder, eq. 18, to two dimensions, where each block is updated following its four neighboring blocks. The generalization of eq. 21 to this case is given by

$$\hat{P}(B_{i,j-1}, B_{i-1,j}, B_{i,j}, B_{i+1,j}, B_{i,j+1}) \equiv \frac{1}{L_0^2} \sum_{i,j}^{L_0} \prod_{k+m=-1,0,1} \delta_{A_{i+k,j+m}, B_{i+k,j+m}} \quad (23)$$

where $L_0^2 = (L/k_0)^2$ is the number of blocks of the two-dimensional array of bits, and again periodic boundary conditions are assumed. Similarly to eq. 21, the dynamical posterior probabilities now take the following form

$$\gamma_n^{B_{k,m}} = \sum_{i,j,s,t=1}^q \frac{\hat{P}(B_i, B_j, B_{k,m}, B_s, B_t)}{\sum_{b=1}^q \hat{P}(B_i, b, B_j)} \times q_{k-1,m}^i q_{k,m-1}^j q_{k+1,m}^s q_{k,m+1}^t \quad (24)$$

It is clear that the generalization of this decoder to a higher dimension is straightforward and in the naive decoding the complexity of the decoder scales as $L_0^d q^{2d-1}$. Nevertheless, similarly to the Markovian joint S/C decoder also in the higher dimensional case the complexity can be reduced and, for instance, in two dimensions

$$\hat{P}(B_{i,j-1}, B_{i-1,j}, B_{i,j}, B_{i,j+1}, B_{i+1,j}) = \frac{\hat{P}(B_{i,j-1}, B_{i,j}) \hat{P}(B_{i-1,j}, B_{i,j}) \hat{P}(B_{i,j+1}, B_{i,j}) \hat{P}(B_{i+1,j-1}, B_{i,j})}{\hat{P}(B_{i,j})^3} \quad (25)$$

and similarly in higher dimensions. Hence, the complexity of a message passing in d dimensions is reduced to $(L_0)^d q^2$, or alternatively the complexity per block is of the order of $O(q^2)$.

Besides the above simplification, it is important to note that for finite L the tensor of the probabilities of occurrence of nearest blocks, for instance eq. 25, for the two-dimensional case, is expected to be very sparse. Hence, the decoder can be accelerated as was discussed for the one-dimensional case.

From an analytical point of view, we do not have an effective way to generate an ensemble of arrays with a given set of autocorrelations in two or higher dimensions, since we do not know how to derive the effective interactions, eq. 7. From a practical point of view, for a given two-dimensional picture and k_0 , we can measure the correlations, eq. 25, and then apply the Markovian decoder. However, there is no reference point to compare the efficiency of the decoder, since we do not have an effective way to calculate the entropy, H_2 , and then Shannon's lower bound, eq. 6, for a given set of correlations in more than one dimension. Practically, the performance of the Markovian decoder in higher dimensions can be compared to other known efficient lossless compression methods for two and higher dimensions. This important comparison certainly warrants further research.

XII. CONCLUDING REMARKS

The only remaining major drawback of the presented Markovian joint S/C coding is that the complexity of the decoder scales in the leading order for large q per message passing as $O(Lq^2/\log_2(q))$.

We note that asymptotically the complexity of the Markovian joint S/C decoder per message passing might be reduced to $O(Lq \log(q))$. The main idea can be exemplified in the framework of the original SM scheme, eq. 10. The complexity of the calculation of each γ_n^c is of the order of q , and it is required to calculate such q different elements. Each summation in eq. 10 consists of the following two types of terms. The first one is the static terms, $S_L(l, c)(S_R(c, r))$, which are the Boltzmann factors, or a row of the transition matrix of the Markov process. The second type is the dynamical posterior probabilities for the neighboring blocks, q_L^l, q_R^r . The static terms can be ordered in a decreasing rank order only once, in the initial stage of the decoder, and the first $O(\log(q))$ largest dynamical posterior probabilities can be found at the cost of $O((q \log(q)))$ per block. Next we run the usual decoder, eq. 10, in one of the following two options: (a) the summations in eq. 10 are done only on the *current* leading $O(\log(q))$ of the dynamical block posterior probabilities, or alternatively (b) the summations are done as was proposed in (a) with the additional $O(\log(q))$ leading terms of the static terms, or any combination of (a) and (b).

The idea behind the above procedure is similar to results of section IX, where only a limited degradation in the performance of the Markovian decoder was observed where the transition matrix was approximated by the knowledge of only a small number dominated terms. Similarly in the presented approximation, we expect that most of the bits are correctly ordered by the dominated part of the static Boltzmann weights and by the dominated part of the dynamical block posterior probabilities. In the final stage of the decoder, rare events of a pair of blocks, small Boltzmann factors, will be correctly ordered by the dominated true posterior block probabilities for one of its two neighbors.

The question which remains to be answered is the origin of the suggested scaling of the order of $O(\log(q))$ dominated taken terms in the summations of eq. 10. The explanation is based on the characteristic features of random graphs [44,45]. In the full operation of the Markovian process one assigns for each pair of nearest blocks a dynamical transition matrix of size $q \times q$, which resembles a fully connected graph consisting of q nodes. The purpose of our approximation is to replace the fully connected graph with the diluted one, *but the graph has still to be connected*; the maximal component of the graph must be q . The lack of finite components is a necessary condition, since in such an event the enhancement of the true block posterior probability may be dynamically forbidden, since there are isolated nodes (states). From the random graph theory it is known that the maximal component is equal to q where the average connectivity (the average number of non-zero transitions per row) is of the order of $O(\log(q))$ [44,45]. This prediction has still to be confirmed in large scale simulations, large L and q .

Finally, note that for large q the transition matrix, $\hat{P}(A, B)$, is a very sparse matrix in the limit $q^2 \gg L$. This limit is achieved even for very large source messages and short-range correlation length, for instance, $k_0 = 12$, $q = 2^{k_0} = 2048$ and $L = 10^5$. Furthermore, in the limit where the number of possible different blocks $q = 2^{k_0} \gg L$, a large fraction of γ_n^c , eq. 10, can be taken as zero probabilities. Hence, the complexity of the decoder can be simplified further by these two effects.

ACKNOWLEDGMENT

I.K thanks David Forney, Wolfgang Kinzel, Manfred Opper, Shlomo Shamai, Rudiger Urbanke and Shun-ichi Amari for many helpful discussions and comments.

-
- [1] Sae-Young Chung, Forney GD Jr, Richardson TJ, Urbanke R, On the design of low-density parity-check codes within 0.0045 dB of the Shannon limit. *IEEE, Communications Letters*, vol.5, no.2, Feb. 2001, pp.58-60.
 - [2] Richardson TJ, Urbanke R, The capacity of low-density parity-check codes under message-passing decoding. *IEEE Transactions on Information Theory*, vol.47, no.2, Feb. 2001, pp.599-618.
 - [3] Luby MG, Mitzenmacher M, Shokrollahi MA, Spielman DA, Analysis of low density codes and improved designs using irregular graphs. *Proceedings of the Thirtieth Annual ACM Symposium on Theory of Computing. ACM. 1998, pp.249-58. New York, NY, USA.*
 - [4] Kanter I, Saad D, Error-correcting codes that nearly saturate Shannon's bound, *Physical Review Letters*, vol.83, no.13, 27 Sept. 1999, pp.2660-3.
 - [5] Berrou C, Glavieux A, Thitimajshima P, Near Shannon limit error-correcting coding and decoding: Turbo-codes. *ICC '93 Geneva. IEEE International Conference on Communications '93. IEEE. 1993, pp.1064-70 vol.2.*, and Berrou C, Glavieux A. Near optimum error correcting coding and decoding: turbo-codes. *IEEE Transactions on Communications*, vol.44, no.10, Oct. 1996, pp.1261-71.

- [6] Shannon CE, A mathematical theory of communication, *Bell System Technical J.*, **27**, 379-423, 623-656, 1948.
- [7] Cover TM, Thomas JA. *Elements of information theory*. Wiley. 1991, UK.
- [8] Michelson, AM and Levesque, AH, *Error-Control Techniques for Digital Communications*, Wiley, New York, 1985.
- [9] Frey BJ, *Graphical Models for Machine Learning and Digital Communication* (MIT Press), 1998.
- [10] Kliever J, Thobaben R, Combining FEC and optimal soft-input source decoding for the reliable transmission of correlated variable-length encoded signals. *Proceedings DCC 2002. Data Compression Conference. IEEE Comput. Soc. 2002, pp.83-91. Los Alamitos, CA, USA*.
- [11] Shamai S, Verdu S, Capacity of channels with uncoded side information. *European Transactions on Telecommunications & Related Technologies*, vol.6,no.5, Sept.-Oct. 1995, pp.587-600.
- [12] Liveris A, Xiong Z and Georgiades CN, Compression of Binary Sources with Side Information Using Low-Density Parity-Check Codes, *Proceedings of Globecom 2002, Taipei, Taiwan, November 17-21 2002*.
- [13] Garcia-Frias J and Villasenor JD, Joint Turbo Decoding and Estimation of Hidden Markov Sources *IEEE J. Sel. Areas Commun.*, Vol. 19, No. 9, pp. 1671-1679, Sept. 2001.
- [14] C.-C. Zhu and F. Alajaji, Turbo Codes for Non-Uniform Memoryless Sources over Noisy Channels, *IEEE Communications Letters*, Vol. 6, No. 2, pp. 64-66, February 2002.
- [15] Garcia-Frias J, Zhao Y, Compression of binary memoryless sources using punctured turbo codes, *IEEE Communication Letters*, vol.6, no.9, pp.394396 (2002).
- [16] Kanter I, Saad D, Finite-size effects and error-free communication in Gaussian channels. *Journal of Physics A-Mathematical & General*, vol.33, no.8, 3 March 2000, pp.1675-81.
- [17] Kanter I and Kfir H, Statistical mechanical aspects of joint source-channel coding, *Europhys. Lett.* Vol. 63 No. 2 pp. 310 (July 2003).
- [18] Kanter I and Rosemarin H, (cond-mat-0301005).
- [19] Sourlas N, Spin-glass models as error-correcting codes. *Nature*, vol.339, no.6227, 29 June 1989, pp.693-5.
- [20] Sourlas N, Statistical mechanics and capacity-approaching error-correcting codes. *Physica A*, vol.302, no.1-4, 15 Dec. 2001, pp.14-21.
- [21] Ein-Dor L, Kanter I, Kinzel W, Low autocorrelated multiphase sequences. *Physical Review E*, vol.65, no.2, Feb. 2002.
- [22] We thank Wolfgang Kinzel for his advice to simplify the decoder by using the Markovian process.
- [23] R. Baxter J, "Exactly Solved Models in Statistical Mechanics", Academic Press, London, 1982.
- [24] I. Kanter, The equivalence between discrete-spin Hamiltonians and Ising Hamiltonians with multi-spin interactions, *J. Phys. A*, vol. 20 pp. L257 1987.
- [25] MacKay DJC and Neal RM, Near Shannon limit performance of low density parity check codes. *Electronics Letters*, vol.33, no.6, 13 March 1997, pp.457-8; MacKay DJC, Good error-correcting codes based on very sparse matrices. *IEEE Transactions on Information Theory*, vol.45, no.2, March 1999, pp.399-431.
- [26] Davey MC and MacKay DJC, Low-density parity check codes over GF(q). *Communications Letters*, vol.2, no.6, June 1998, pp.165-7.
- [27] Nakamura K, Kabashima Y and Saad D, Statistical mechanics of low-density parity-check codes over Galois fields, *Europhys. Lett.*, vol. 56, 2001, pp. 610-616.
- [28] MacKay D. J. C, Wilson S. T. , Davey M. C. Comparison of constructions of irregular Gallager codes. *IEEE Transactions on Communications*, vol.47, no.10, Oct. 1999, pp.1449-54. Publisher: IEEE, USA M.C. Davey and D.J.C. MacKay, *IEEE Comm. Lett.*, in press (1999).
- [29] MacKay DJC and Davey MC, *Gallager Codes for Short Block Length and High Rate Applications, Codes, Systems and Graphical Models*, IMA Volumes in Mathematics and its Applications, Springer-Verlag (2000).
- [30] Kabashima Y, Saad D, Statistical mechanics of error-correcting codes. *Europhysics Letters*, vol.45, no.1, 1 Jan. 1999, pp.97-103.
- [31] Skantzos NS, van Mourik J, Saad D and Kabashima Y, Average and reliability error exponents in low-density-parity-check-codes, *J. Phys. A* (in press).
- [32] Gallager RG, *Low density parity check codes* Research monograph series **21** (MIT press), 1963.
- [33] Priel A, Blatt M, Grossman T, Domany E, Kanter I, Computational capabilities of restricted two-layered perceptrons. *Physical Review E*, vol.50, no.1, July 1994, pp.577-95.
- [34] In practice we define t_{med} to be the average convergence time of all samples with $t \leq$ the median time.
- [35] For rate 9/8, for instance, the chosen construction for the matrices A and B are as follows. For A , the fraction of rows (from the first row of A) (1/16, 1/4, 9/16, 1/16, 1/16) are characterized by 1, 2, 3, 5, 9 non-zero elements per row, respectively. The structure of B is the same as illustrated in Fig. 2, but 1.75 is replaced with 7/9. We ran simulations for this construction with $C_1 = C_2 = 0.7$ and the corresponding entropy is $H_2 = 0.513$ and $L = 9,000$. The extrapolation of t_{med} indicates that the threshold of this code for large L is $f_c \sim 0.057$. In the separation scheme using *optimal compression and error correction schemes* and with $f_c = 0.057$ ($R_{i.i.d} = 0.618$), one can find that the overall inverse rate of the communication channel is $1/R = 0.513/0.618 \sim 0.83$, which is only about 6% below our joint S/C inverse rate $1/R = 8/9 \sim 0.89$. One must remember that our MN construction can be further optimized, and the critical channel noise is expected to be enhanced, $f_c > 0.057$.
- [36] The PPMZ software used can be downloaded from www.cbloom.com/src/ppmz.html
- [37] The AC software used can be downloaded from www.cs.mu.oz.au/~alistair/arith_coder

- [38] A similar degradation in the performance was observed for $q = 2$ and biased binary messages (each source bit is equal 0/1 and is chosen with probability $p/1 - p$). As $|p - 0.5|$ increases the entropy decreases and a degradation in the performance of the MN algorithm was observed.
- [39] Kfir H and Kanter I (unpublished).
- [40] Shahar K and Kanter I (unpublished).
- [41] McLachlan GJ and Krishan T, The EM Algorithm and Extension. *Wiley Sons, New York, 1997*.
- [42] I. Kanter thanks Manfred Opper for the discussion and the explanations of this general result
- [43] In principle one can generalize the tensor to include nearest and next-nearest blocks.
- [44] Erdos P and Reyni A, "The Art of Counting", Edit. by J. Spencer (MIT Press, Cambridge MA , 1973).
- [45] Kanter I, Sompolinsky H. Mean-field theory of spin-glasses with finite coordination number. *Physical Review Letters*, vol.58, no.2, 12 Jan. 1987, pp.164-7.